Human replication licensing factor Cdt1 directly links mitotic kinetochores to spindle microtubules

Shivangi Agarwal[1], Kyle Paul Smith[1], Yizhuo Zhou[2], Aussie Suzuki[3], Richard James McKenney[4], Dileep Varma[1*]

[1]Department of Cell and Molecular Biology, Feinberg School of Medicine, Northwestern University, 303 E Chicago Avenue, Chicago, Illinois 60611, USA

[2]Department of Biochemistry and Biophysics, The University of North Carolina at Chapel Hill, Chapel Hill, NC 27599, USA

[3]Department of Biology, The University of North Carolina at Chapel Hill, Chapel Hill, NC 27599, USA

[4]Department of Molecular and Cellular Biology, University of California-Davis, 145 Briggs Hall, Davis, California 95616, USA

[1]*Corresponding author: dileep.varma@northwestern.edu

Running title: Cdt1 binds to microtubules

Cdt1, a new kinetochore microtubule-binding protein

Short summary

- Cdt1 binds and diffuses on microtubules
- The winged-helix domain at the C-terminal region of Cdt1 is involved in MT-binding
- Aurora B Kinase phosphorylates Cdt1 and influences its MT-binding
- Aurora B-mediated Cdt1 phosphorylation is necessary for kMT stability and mitotic progression

Abstract

Robust kinetochore-microtubule (kMT) attachment is critical for accurate chromosome segregation. G2/M-specific depletion of human Cdt1, a protein that localizes to kinetochores in an Ndc80 complex-dependent manner, leads to abnormal kMT attachments and mitotic arrest indicating an independent mitotic role for Cdt1 in addition to its prototypic DNA replication origin licensing function. Here, we show that Cdt1 directly binds to microtubules (MTs). Transiently expressed Cdt1 localizes to mitotic spindle MTs. Deletion mapping revealed that the C-terminus of Cdt1 carrying a winged-turn-helix domain is necessary but not sufficient for MT-binding. Mitotic kinase Aurora B interacts with and phosphorylates Cdt1. Aurora B-phosphomimetic Cdt1 exhibited attenuated MT-binding and its cellular expression induced defective kMT attachments and mitotic progression. Thus we provide evidence for a Cdt1-mediated MT-attachment site at kinetochores. We propose that Cdt1 links the loop domain of Ndc80 to MTs and enables an optimal MT-binding state for the complex.

Introduction

Accurate chromosome segregation during mitosis is accomplished by the concerted function of the bipolar mitotic spindle and kinetochores (Westhorpe and Straight, 2013). In this process, mitotic cells inevitably confront a challenge to maintain the kinetochore-microtubule (kMT) attachment robust enough to prevent unwarranted detachments owing to the dynamic instability generated by rapid polymerization (growth) and depolymerization (shrinkage) of microtubules (MTs) (DeLuca and Musacchio, 2012; Joglekar et al., 2010). How this dynamic process of kMT coupling is accomplished and regulated in vertebrates is not well understood.

A highly conserved network of protein complexes, called the KMN network (Knl1, Mis12, Ndc80) is the core interface that links spindle MTs to the kinetochores (Afreen and Varma, 2015; Cheeseman et al., 2006; Cheeseman and Desai, 2008). The N-terminal region of the Ndc80 complex, containing the Calponin homology (CH) domain and positively charged tail domain of the Hec1 subunit, constitute MT-binding site (Varma et al., 2012). The N-terminal region of Knl1 has also been shown to be necessary for MT binding (Cheeseman et al., 2006; Espeut et al., 2012; Welburn et al., 2010). Recently, an unprecedented mitotic role for human Cdt1 was discovered in addition to its well-established role in licensing DNA replication origins (Varma et al., 2012); (Pozo and Cook, 2016). The Hec1 loop domain that generates a flexible hinge in an otherwise rigid Ndc80 (Wang et al., 2008), has been shown to recruit Cdt1 to kinetochores by interacting with the N-terminal region of Cdt1 (Varma et al., 2012). Precise high-resolution separation measurement (delta) analysis between the extreme N- and C-termini of Ndc80 revealed that the Ndc80 complex bound to Cdt1 maintains an extended conformation that served

to stabilize kMT attachments by a mechanism, the details of which are obscure. However, in the absence of Cdt1, the coiled coil of the Ndc80 complex was bent producing delta measurements of only ~68-76% compared to normal metaphase cells (Varma et al., 2012). Thus, while substantial research has provided insights into the structural and mechanistic aspects of the "*canonical*" licensing function of Cdt1, how Cdt1 influences kMT attachments during mitosis remains unclear.

Besides Cdt1, the loop region of Hec1 also serves as a docking site for several other microtubule-associated proteins (MAPs) such as Dis1 (vertebrate homolog of chTOG) and Dam1 in yeast (Hsu and Toda, 2011; Maure et al., 2011; Schmidt and Cheeseman, 2011). In fact, in budding yeast, the Ndc80 and Dam1 complexes function synergistically to bind to MTs (Tien et al., 2010). Similarly, in vertebrates the loop region has been reported to recruit the Ska complex (Zhang et al., 2012) that not only interacts with MTs through the C-terminal domain of Ska1 [which adopts a unique winged-helix fold (WTH)] but the Ndc80 complex increases the affinity of the Ska1 subunit for MTs by 8-fold (Abad et al., 2014; Schmidt et al., 2012). These studies suggest that although the Ndc80 complex is critical for kMT-binding, other factors such as the Dam1 and Ska complexes are required to efficiently orchestrate kMT attachments and chromosome segregation.

The present study was thus undertaken to address critical outstanding questions in the context of our previous study that illustrated a role for Cdt1 at kinetochores in stabilizing kMT attachments (Varma et al., 2012). These include: (1) whether Cdt1 directly binds to MTs, and (2) how Cdt1 is regulated for its mitotic function. Employing several biochemical, biophysical and cell biological approaches, we demonstrate that human

Cdt1 can directly interact with MTs, and we characterize the Cdt1-MT binding parameters in-depth. We further show that Cdt1 is a novel target for Aurora B Kinase (ABK) and that phosphorylation by ABK regulates the MT-binding properties of Cdt1 to influence normal mitotic progression.

Results and discussion

Cdt1 directly binds to microtubules *in vitro*

Using a novel RNAi-mediated knockdown approach and microinjection of a function-blocking Cdt1 antibody, we previously demonstrated that perturbation of Cdt1 function specifically during mitosis led to unstable kMT attachments culminating in a late prometaphase arrest (Varma et al., 2012). Based on these observations, we posit a new paradigm where Cdt1 bound to the loop provides a direct link to MTs to create an additional MT-attachment site for the Ndc80 complex and helps extend the Ndc80 complex along the axis of kMTs to bind MTs more robustly.

To test our hypothesis, we assessed the ability of purified human Cdt1 to bind to MTs directly. Since no high-resolution structures of full-length Cdt1 have been published, we first subjected the human Cdt1 amino acid sequence to at least ten different secondary structure prediction algorithms that predict disordered regions. Although, the consensus readily identified previously crystallized winged helix domains (WHD) as being well-folded; the N-terminal 93 amino acids were convincingly predicted to be at least ~35% intrinsically disordered, in addition to the “linker” region between the two WH domains **(Fig. 1 A)** even with very stringent cutoffs. Homology models generated using three modeling programs, reliably identified the middle (WHM) and the C-terminal winged helix

domains (WHC), while the N-terminal region (1-160) was consistently predicted to have only limited secondary structure elements in the absence of other binding partners **(Fig. 1 B)**. The NMR solution structure (PdbID: 2KLO) determined for the C-terminal 420-557 aa of *Mus musculus*, abbreviated as mCdt1, revealed that this region adopts a winged-helix-turn-helix fold/domain (WTH/WHD) (Khayrutdinov et al., 2009) in addition to the other WHD in the middle domain of Cdt1 (172-368 aa) responsible for Geminin binding (Lee et al., 2004). The WHD has traditionally been implicated primarily as a DNA binding motif, but emerging evidences suggest that it could also serve as a protein-protein interaction domain (Khayrutdinov et al., 2009). In addition to the canonical three helix-bundles and anti-parallel beta-sheets, the Cdt1 WHC also contains an additional helix (H4) at the C-terminus (**Fig. S1 A**). Superimposition of the homology model for human Cdt1 fragment 410-546 aa [generated using Phyre2 (Kelley et al., 2015)] with the available NMR structure of an mCdt1 fragment showed an overlap with the root mean square deviation of 1.038 Å, indicating that the 410-546 aa of human Cdt1 also conforms to a WTH domain (**Fig. 1 B**).

Proteins with large disordered regions are generally characterized by rapid degradation (Vavouri et al., 2009). Indeed, challenges in purifying the full-length human Cdt1 from bacterial system were circumvented by the deletion of the 92 aa disordered stretch from its N-terminus which likely contributed to its degradation, reduced expression and poor solubility. This major Cdt1 fragment (92-546 Cdt1) was successfully purified with an N-terminal GFP fusion (**Fig. 1, C and D**) and was evaluated for its ability to bind to MTs in a co-pelleting assay. The 92-546 Cdt1 (1 μM) was found to co-pellet efficiently with taxol-stabilized MTs (**Fig. 1 E**). This interaction with MTs is specific as Cdt1 was

barely (~10%) detected in the pellet fraction in the absence of MTs. To determine the apparent MT-binding affinity of 92-546 Cdt1, we varied the MT concentration and measured the Cdt1 concentration required for half maximal binding. In this assay, the affinity was computed to be 2.20 ± 0.87 µM (**Fig. 1 F**) which is comparable to other relevant kinetochore MAPs such as chTOG (Spittle et al., 2000), Ska (Schmidt et al., 2012), the KMN network and the Ndc80 complex (Cheeseman et al., 2006; Ciferri et al., 2008) determined using similar approaches. Since the construct used in this assay was devoid of the first 92 aa, full-length (FL) Cdt1 (1-546 aa) was purified with a GST tag which was subsequently cleaved using Factor Xa and the tagless FL-Cdt1 was tested for its ability to bind to MTs. As expected, the full-length protein also bound to MTs (**Fig. 1 E**) with an affinity (2.29 ± 0.45 µM) akin to the 92-546 Cdt1 (**Fig. 1 F)**; indicating that the first 92 aa are dispensable for the MT binding function of Cdt1. In further support of this, a degraded variant of full length GST-Cdt1 (abbreviated as GST-ΔC) that retained its N-terminal GST tag along with the first 92 aa but lacked ~100-150 aa from the C-terminus (assessed using antibodies; **Fig S1 B**), did not bind to MTs (**Fig. 1 E**). As controls, neither purified GFP nor GST proteins fractionated with MTs substantiating the specificity of interaction **(Fig. S1, C and D)**.

To map the Cdt1-MT interaction, deletion fragments within 92-546 Cdt1 were generated as GFP chimeras (**Fig. 1, C and D**). Interestingly, MTs could not sediment either of the N-terminal fragments, 92-232 or 92-410 (**Fig. 1, G and H**). However, the smallest C-terminal fragment 410-546 did show MT binding to a greater extent in comparison to the other fragments, albeit its efficacy was reduced by ~50% as compared to 92-546 Cdt1 (**Fig. 1 I**). This is similar to and is reminiscent of the observation with the

Ska complex, wherein the removal of C-termini from either Ska1 or Ska3 impaired MT binding. At the same time, the purified C-terminal domains of Ska1 or Ska3 by itself did not associate with MTs (Jeyaprakash et al., 2012). This suggests that the N-terminus of Cdt1 may be inert for MT binding by itself but might facilitate the folding or positioning of the C-terminus of Cdt1 to allow its MT binding function. Thus, we conclude that the C-terminus of Cdt1 (410-546 aa) is necessary but not sufficient for MT binding. We predict that the C-terminal (WHC) or centrally located (WHM) domains may be required in combination for efficient binding of Cdt1 to MTs. These observations also suggest that the WHD domain could serve as one of the conserved MT-binding domains in MT-binding proteins as has already been demonstrated for the Ska complex (Abad et al., 2014).

Cdt1 preferentially binds to straight MTs independent of the E-hook tails

At the C-terminus of tubulin are negatively charged acidic tails of ~20 aa, known as "E-hooks" that represent a critical recognition site for many proteins that bind to MTs including Ndc80^{Bonsai} (Ciferri et al., 2008) and Dam1 (Ramey et al., 2011). The ability of Cdt1 to bind to subtilisin-treated MTs devoid of E-hooks was thus assessed in a co-sedimentation assay (**Fig. 2, A and B**). Similar to Ska1 (Abad et al., 2014) and chTOG (Spittle et al., 2000), 92-546 Cdt1 did not show any appreciable reduction in its ability to bind to MTs without the acidic tail (**Fig. 2, A and B**). This suggests that the critical contacts involved in this interaction might be the structured regions of tubulin monomers rather than just the acidic tails. The highly basic nature of Cdt1 (predicted pI=9.9) is indicative of MT recognition through electrostatic/ionic interactions. Indeed, the binding of 92-546

Cdt1 with MTs was substantially reduced to ~50% in the presence of 250 mM NaCl (**Fig. 2 C**); suggesting that the binding may be at least partially electrostatic in nature.

Further, we assessed the preference for Cdt1 to bind to straight *vs* curved MTs. Unlike the CH domains of Ndc80 that bind to the dimeric tubulin interface and prefer a straight MT protofilament conformation; Ska accesses MTs by interacting with the structured regions within tubulin monomers independent of any conformation (Abad et al., 2014). The data revealed that even though MT-binding was considerably reduced when the MTs were not straight; Cdt1 did retain the capacity to bind to curved MT protofilaments (**Fig. S2, B and C**), which might have important implications for the function of Cdt1 at the kMT interface in conjunction with the Ndc80 complex.

In order to test the preference of Cdt1 to bind to MT ends, polymerized MTs were sheared to increase the number of ends. We did not observe any significant increase in the association of Cdt1 with the MTs in this scenario (**Fig. S2, B and C**). This suggests that Cdt1 might not be merely a MT plus/minus end-specific protein, but its binding sites are likely distributed along the length throughout the MT lattice.

Cdt1 diffuses on MTs *in vitro* and decorates spindles *in vivo*

To substantiate Cdt1-MT binding further, we directly visualized single molecules of GFP-92-546 Cdt1 interacting with MTs using total internal reflection fluorescence microscopy (TIR-FM). The 92-546 Cdt1 showed binding to the Dylight405-labelled MTs at concentrations as low as 1 nM (**Fig. 2 D)** and at a higher concentration (10 nM or higher), it completely decorated the entire MT lattice **(Fig. S2 D)**. In our conditions, individual molecules either bound statically or diffused along the MT lattice **(Fig. 2 E)**. The dwell

time distribution for 92-546 on MTs was well described by a single exponential decay function yielding a characteristic dwell time (τ) of 2.37 sec **(Fig. 2 F)**. The calculated association rate (K_{on},10^{-6},s^{-1},nM^{-1}) was 1.07 ± 0.38 and the dissociation constant (K_D, μM) was 0.46 ± 0.17 (**Fig. 2 F**). A large fraction of 92-546 (~65%) was found to undergo short-range diffusive motion along the MT lattice to a moderate extent that falls in the range of 0-0.5 μm^2/sec **(Fig. 2 G)**, as depicted in the kymographs (**Fig. 2 E**) and in the supplemental movie (**Movie S1**). A smaller fraction (~20%) did not apparently diffuse at all while an even smaller fraction (~15%) exhibited relatively fast diffusion (>1 μm^2/sec). The average diffusion coefficient for 92-546 was ~0.16 μm^2/sec under our experimental conditions (**Fig. 2 G**). Both Ndc80 and Ska complexes have also been shown to exhibit diffusion along the MT lattice; albeit at variable rates comparable to that observed for Cdt1 under our assay conditions. The GFP-hSka1/2 and hNdc80 "Broccoli"-GFP exhibited diffusion on MTs with D=0.18 μm^2/s and 0.03 μm^2/s, respectively (Schmidt et al., 2012). Using "Bonsai" Ndc80-GFP, this value was D=0.078 μm^2/sec (Zaytsev et al., 2015).

Although the *in vitro* experiments provide conclusive evidence that Cdt1 binds to MTs, we sought evidence for this activity in cells. We had previously observed Cdt1 localization at mitotic kinetochores in paraformaldehyde-fixed LLCPK1 and Ptk2 cells (Varma et al., 2012). We now show Cdt1 localization to kinetochores in HeLa cells using identical fixation conditions (**Fig. 2 H, bottom panels**). When we performed immunofluorescence staining of Cdt1 in methanol-fixed HeLa cells, which removed most of the kinetochore staining, we were able to visualize clear mitotic spindle staining (**Fig. 2 H, top panels)**. To lend further support to these observations, full-length Cdt1 was

transiently over-expressed with an HA tag in HeLa cells and immunostaining was performed to assess its localization. In agreement with the results so far, staining with anti-HA clearly reveals localization of Cdt1-HA on the spindle MTs and also on kinetochores (overlap with Hec1, a kinetochore marker required for Cdt1 recruitment) in mitotic cells (**Fig. 2 J, top panels**). As shown in the Fig. 2 K, magnification of selected kinetochores from multiple cells further validates Cdt1 localization to kinetochores and kMTs. Strikingly, many interphase cells expressing Cdt1 showed a MT bundling phenotype (**Fig. 2 J**), similar to what was observed with GFP-Ska1 over-expression (Welburn et al., 2009). Moreover, in cells that were undergoing cytokinesis, Cdt1 was localized to MT-bundles at the mid-body region (**Fig. 2 J**). Western blotting of transfected HeLa cell lysates with anti-HA (representing the exogenously expressed Cdt1 with HA tag) and anti-Cdt1 (for endogenous Cdt1) antibodies showed the migration of Cdt1 at ~60 kDa (**Fig. 2 L**), confirming its expression as full-length protein in fusion with the HA tag. Similar MT-staining (spindle/spindle pole) was also obtained in HeLa cells that stably expressed HA-tagged Cdt1, representing a scenario between over- and endogenous expression (**Fig. 2 I**).

Aurora B Kinase (ABK) phosphorylates Cdt1 and affects Cdt1-MT binding *in vitro*

ABK phosphorylates multiple substrates at kinetochores to negatively regulate kMT attachments and is also instrumental in correcting erroneous attachments (Chan et al., 2012; Schmidt et al., 2012; Welburn et al., 2010). *In vitro* studies with purified Ndc80 complex demonstrated that introduction of either multiple phosphorylations or phosphomimetic substitutions within the Hec1 tail reduced Ndc80-MT binding, while a

lack of phosphorylation promoted stronger binding (Cheeseman et al., 2006; Umbreit et al., 2012). Similarly, Ska1, another kinetochore-localized MAP is a substrate for ABK and its phosphorylation at four sites located within the MTBD drastically reduces its kinetochore localization (Chan et al., 2012; Schmidt et al., 2012; Welburn et al., 2010). Mutating two of these, S185 and S242 to aspartate dramatically reduced the MT binding activity of the Ska complex *in vitro* and resulted in a mitotic delay and reduced kMT stability *in vivo* (Chan et al., 2012; Schmidt et al., 2012; Welburn et al., 2010). Recently, Ska3 has been shown to undergo Cdk1-mediated phosphorylation during mitosis that influences its interaction with the Ndc80 loop domain; which is in turn proposed to affect the recruitment of Ska complex at the kinetochores and facilitate Ska1 binding to MTs (Zhang et al., 2017). These afore-mentioned studies thus propound a strong evidence in favor of phosphoregulation of MT-binding kinetochore proteins; which prompted us to question if Cdt1-MT binding is similarly phosphoregulated.

Cdt1 has previously been shown to be phosphorylated by Cyclin-dependent kinase 1 (Cdk1) during S-phase at Threonine 29 (Fujita, 2006) and by Mitogen-activated protein (MAP) kinases p38 and c-Jun N-terminal kinase (JNK) during G2/M phase (Chandrasekaran et al., 2011). The five MAPK sites are located towards the C-terminus of Cdt1 close to the predicted/mapped MT-binding WTH domain (410-546 aa); mutating these five residues in Cdt1 to generate a GFP-tagged-phosphomimetic (92-546-2E3D; S391D, T402E, T406E, S411D, S491D) did not however impact the MT-binding ability *in vitro* (data not shown). This led us to insinuate that another kinase might be involved in regulating Cdt1-MT binding in mitosis.

A close examination of the Cdt1 sequence revealed at least 7 Aurora B phosphorylation sites (T7, S73, S101, T102, S143, S265, T358) organized in a canonical ABK consensus motif [$(R/K)_{1-3}$-X-(S/T)] (Meraldi et al., 2004) **(Fig. 3 A)**. Five of these seven sites (S73, S101, T102, S143 and S265) have been reported as phosphorylation sites in the literature-curated database (www.phosphosite.org and www.phosida.org). Interestingly, 3 other potential sites (T270, T287 and T329) that albeit did not conform to the classical ABK sequence motif but were considered in our analysis. Firstly, because they were conserved across the species **(Fig. 3 A)** and secondly, highly conserved S159 in Ska3 arranged as "QLS" that also did not match the canonical Aurora B consensus was shown to be clearly phosphorylated by ABK (Chan et al., 2012). In light of these observations and the well-established role of ABK in regulating kMT attachments, we hypothesized a possible role for ABK in regulating Cdt1-MT-binding. To validate this hypothesis, we first sought to test if Cdt1 is a substrate for ABK using an *in vitro* phosphorylation assay. Under the assay conditions, both myc-tagged full-length hekCdt1 (purified from HEK 293 cells and procured commercially) and Vimentin [an established ABK substrate (Goto et al., 2003)] were readily phosphorylated by ABK **(Fig. 3 B)**. This phosphorylation was markedly reduced upon addition of ZM447439, an ABK inhibitor, attesting to its specificity. In tandem, Aurora B kinased hekCdt1 (using a non-radioactive ATP) was subjected to mass-spectroscopy for identification of phosphosites. The MS/MS spectra conclusively detected phosphorylation on four ABK consensus sites *viz* T7, T102, S143, and T358 uniquely/exclusively in the kinase treated hekCdt1 with 90% sequence coverage in two independent runs **(Fig. S3)**. S73 and T270 were detected as phosphorylated even in the unkinased control hekCdt1; suggesting that these residues

can potentially acquire phosphorylation *in vivo*. While the S101 and S265 were found to be localized on the peptides that were phosphorylated, the exact modified residues could not be designated. The remaining 2 non-canonical sites T287 and T329 were identified as unmodified.

Interestingly, Ni^{+2}-NTA agarose-mediated affinity precipitation of HA/His-tagged Cdt1 (from thymidine synchronized and nocodazole-arrested mitotic cell extracts), but not GFP, led to the co-precipitation of ABK as an interacting partner (**Fig. 3 C**). Moreover, ABK was also co-precipitated with the HA-tagged T29A-Cdt1 equally efficiently as with the wild-type Cdt1; implying that the interaction between Cdt1 and ABK in mitosis is independent of Cdk1-phosphorylation (**Fig. 3 C**).

Upon mutating the 8 putative Aurora B Ser/Thr residues (8D) to Asp in 92-546 Cdt1 in an attempt to mimic constitutively phosphorylated Cdt1 **(Fig. 3 D)**, we observed ~2.5 fold reduction in the apparent MT binding as evidenced by an increase in the K_d from 2.03 ± 0.99 µM for the 92-546 Cdt1 to 5.50 ± 2.41 µM for the 8D mutant **(Fig. 3, E and F)**. Substitution of the residues to non-phosphorylatable Ala (8A) did not impact the MT binding with K_d value comparable to the parental 92-546 Cdt1. Intriguingly, the 10 identified putative ABK sites are located within the N-terminal unstructured and central WHD (1-410 aa) of Cdt1 that did not show direct association with MTs but somehow seem to contribute to efficient Cdt1-MT interaction (**Fig. 1, G and I**). Since many of these sites are clustered in regions which are predicted to be disordered, we surmise that ABK phosphorylation might induce a conformational change in Cdt1 to regulate its MT-binding ability. This mode of regulation can exist in addition to or in parallel to the manner in which

ABK phosphorylation generally interferes with electrostatic interactions to modulate the affinity of binding; as observed for the Ndc80 complex.

Aurora B-phosphomimetic mutations in Cdt1 affects kMT stability and mitotic progression

To assess the role of ABK-mediated phosphorylation for Cdt1-MT binding *in vivo*, we investigated the function of the ABK phosphomimetic and non-phosphorylatable Cdt1 mutants in HeLa cells using an experimental strategy that had been established previously. This approach involves siRNA-based knockdown and rescue of Cdt1 function in double thymidine synchronized cells specifically in the G2/M phase of the cell cycle to ensure that Cdt1 function in replication licensing during G1 phase is unperturbed (Varma et al., 2012). We first generated HeLa cells stably expressing HA-tagged wild-type and phosphomutant Cdt1 using a retroviral transduction-based approach. Under our conditions, ~90% knockdown of endogenous Cdt1 was achieved while the expressed siRNA resistant HA-tagged Cdt1 constructs were retained **(Fig. S4 A)**. We first tested the stability of kMTs in cells which were depleted of endogenous Cdt1 but expressed Cdt1 wild-type or phosphorylation site mutants; after exposing them to cold treatment. In endogenous Cdt1-depleted cells, the expression of Cdt1-WT rescued kMT stability as opposed to that of the phosphomimetic mutant (Cdt1-10D) or the vector control (simulates Cdt1-depleted state) (**Fig. 4, A and B**). However, the non-phosphorylatable mutant (Cdt1-10A) not only maintained stable kMT attachments but the quantitation of fluorescence intensities of spindle MTs suggested hyper-stability of kMTs (**Fig. 4, A and B**). The cells

expressing either the WT or mutant proteins after endogenous Cdt1 depletion had apparently normal spindle structures at 37ºC **(Fig. S4 B)**.

Approximately 60% of the cells analyzed in Cdt1-10D and 80% in vector control had no discernible MT structures after cold exposure; in the remaining cells that showed extant MT traces, the MTs were not attached to the kinetochores (**Fig. 4 A**, last panels in each vector and 10D). Quantification of the bi-oriented kinetochores that made contact with cold-stable MTs from opposite spindle poles revealed ~90% decrease in cells expressing phosphomimetic Cdt1 as compared to cells expressing wild-type or phospho-defective Cdt1 (**Fig. 4 C**).

The inter-kinetochore distance (K-K stretch) serves as another indicator of the strength of kMT attachment, and thus was also measured in each case as an additional parameter. The average K-K stretch in cells expressing Cdt1-WT and Cdt1-10A was 1.11 ± 0.09 μm and 1.16 ± 0.15 μm, respectively (**Fig. 4 D**); again implying kMTs from opposite spindle poles forming robust contact with the sister kinetochore pairs. In contrast, the Cdt1-10D mutant exhibited a significant reduction in the distance between the two sister kinetochores (0.73 ± 0.10 μm) similar to the vector control, 0.72 ± 0.08 μm indicating weakened load-bearing kMT attachments between sister kinetochore pairs (**Fig. 4 D**).

Progression through mitosis was also assessed in each case by fixed-cell analysis wherein the cells were fixed at two different time points after release from thymidine arrest; mitotic onset (11.5 h) and anaphase onset (12.5 h) (Varma et al., 2012). The mitotic progression of cells expressing Cdt1-10D was severely disrupted. Similar to that observed for vector control after the depletion of endogenous Cdt1 (Varma et al., 2012), the Cdt1-10D expressing cells exhibited a phenotype resembling a mid to late pro-

metaphase arrest at the latter time point (**Fig. 4, E and F)**, where majority of the cells had chromosomes that were partially aligned around a vaguely defined metaphase plate **(Fig. S4 B)**, while a smaller fraction of cells exhibited substantially higher levels of chromosome mis-alignment **(**data not shown). These phenotypes were strikingly different from the cells expressing the Cdt1-10A mutant, which underwent anaphase onset and cytokinesis normally as did the cells expressing Cdt1-WT. Taken together, these results suggest that Cdt1 phosphorylation by ABK *in vivo* is important for generating stable kMT attachments and normal mitotic progression through anaphase.

Conclusions

In this study, we demonstrate that the DNA replication licensing protein Cdt1, which is recruited to mitotic kinetochores by the Ndc80 complex, also binds to MTs in a manner that is controlled by its phosphorylation by Aurora B Kinase. The behavioral parameters and regulatory aspects of key MT-binding proteins at vertebrate kinetochores shown to have a role in stabilizing kMT attachments are summarized in **Fig. 5A**. Based on our observations, we propose that the kinetochore-localized Cdt1 provides another MT-binding site for the Ndc80 complex at its loop domain, thus shedding light on the importance of Cdt1 and the loop in kMT attachments. We envisage that the loop domain of the Ndc80 complex either alone or in conjunction with bound Cdt1 might also coordinate with other kinetochore MAPs to confer stronger attachments. Thus, future studies will be required to delineate the details of hierarchical recruitment of kinetochore components by the Ndc80 loop. Our work while providing an essential missing link in the series of events that take place during the stabilization of kMT attachments in mitosis

(Fig. 5B), also opens up a number of stimulating questions such as: (a) whether the Ndc80 complex has any synergistic influence on Cdt1 binding to MTs; (b) does Ska and Cdt1 coordinate for robust kMT attachments? if so, do these proteins dock on to the loop as a pre-formed complex or do they interact after they are independently recruited at the loop; (c) can Ska, Ndc80 and Cdt1 generate a ternary complex for efficient MT binding; (d) does chTOG, another Ndc80-recruited kinetochore MAP influence localization of Cdt1 and its interaction with MTs; (e) is there a cross-talk and/or interplay of several other kinases besides ABK to fine-tune the phosphoregulation of Cdt1 in mitosis; (f) how phosphorylation of Cdt1 with one or many mitotic kinases influences its localization to kinetochores and whether it affects recruitment of other kinetochore-associated proteins directly or indirectly? Answers to these questions will have major impact on the mitosis field in the quest for novel mechanisms that link mitotic kinetochores to spindle MTs and drive accurate chromosome segregation.

Acknowledgments

We thank Dr. Jeanette Cook for the HA-tagged Cdt1 expression plasmid and for constructive suggestions; Dr. Sarah Rice for valuable intellectual input and discussions; Dr. Mohammed Amin for reading the manuscript; Dr. Laimonis A Laimins and Kavi Mehta for providing help with the radioactive experiments; Northwestern Genomics Core for DNA sequencing services; Suchithra Seshadrinathan and Dr. Anita Varma for technical support. This work was supported by National Cancer Institute grant R00CA178188 to DV, and National Institutes of Neurological Diseases and Stroke grant R00NS089428 to RJM. The authors declare no competing financial interests.

Author contributions

S.A. and D.V. designed and performed majority of the experiments. K.P.S. purified Cdt1, did structural and computational studies and provided intellectual input. Y.Z. performed the co-immunoprecipitation experiment. R.J.M. performed single molecule TIR-FM experiments. S.A., R.J.M. and D.V. analyzed the data. S.A. and D.V. wrote the manuscript with input from all the authors.

References

Abad, M.A., B. Medina, A. Santamaria, J. Zou, C. Plasberg-Hill, A. Madhumalar, U. Jayachandran, P.M. Redli, J. Rappsilber, E.A. Nigg, and A.A. Jeyaprakash. 2014. Structural basis for microtubule recognition by the human kinetochore Ska complex. *Nature communications*. 5:2964.

Afreen, S., and D. Varma. 2015. Cell Division: Molecular Pathways for KMN Kinetochore Recruitment. *Current biology : CB*. 25:R332-335.

Chan, Y.W., A.A. Jeyaprakash, E.A. Nigg, and A. Santamaria. 2012. Aurora B controls kinetochore-microtubule attachments by inhibiting Ska complex-KMN network interaction. *The Journal of cell biology*. 196:563-571.

Chandrasekaran, S., T.X. Tan, J.R. Hall, and J.G. Cook. 2011. Stress-stimulated mitogen-activated protein kinases control the stability and activity of the Cdt1 DNA replication licensing factor. *Molecular and cellular biology*. 31:4405-4416.

Cheeseman, I.M., J.S. Chappie, E.M. Wilson-Kubalek, and A. Desai. 2006. The conserved KMN network constitutes the core microtubule-binding site of the kinetochore. *Cell*. 127:983-997.

Cheeseman, I.M., and A. Desai. 2008. Molecular architecture of the kinetochore-microtubule interface. *Nature reviews. Molecular cell biology*. 9:33-46.

Ciferri, C., S. Pasqualato, E. Screpanti, G. Varetti, S. Santaguida, G. Dos Reis, A. Maiolica, J. Polka, J.G. De Luca, P. De Wulf, M. Salek, J. Rappsilber, C.A. Moores, E.D. Salmon, and A. Musacchio. 2008. Implications for kinetochore-microtubule attachment from the structure of an engineered Ndc80 complex. *Cell*. 133:427-439.

DeLuca, J.G., and A. Musacchio. 2012. Structural organization of the kinetochore-microtubule interface. *Current opinion in cell biology*. 24:48-56.

Espeut, J., D.K. Cheerambathur, L. Krenning, K. Oegema, and A. Desai. 2012. Microtubule binding by KNL-1 contributes to spindle checkpoint silencing at the kinetochore. *The Journal of cell biology*. 196:469-482.

Fujita, M. 2006. Cdt1 revisited: complex and tight regulation during the cell cycle and consequences of deregulation in mammalian cells. *Cell Div*. 1:22.

Goto, H., Y. Yasui, A. Kawajiri, E.A. Nigg, Y. Terada, M. Tatsuka, K. Nagata, and M. Inagaki. 2003. Aurora-B regulates the cleavage furrow-specific vimentin phosphorylation in the cytokinetic process. *The Journal of biological chemistry*. 278:8526-8530.

Hsu, K.S., and T. Toda. 2011. Ndc80 internal loop interacts with Dis1/TOG to ensure proper kinetochore-spindle attachment in fission yeast. *Current biology : CB*. 21:214-220.

Jeyaprakash, A.A., A. Santamaria, U. Jayachandran, Y.W. Chan, C. Benda, E.A. Nigg, and E. Conti. 2012. Structural and functional organization of the Ska complex, a key component of the kinetochore-microtubule interface. *Mol Cell*. 46:274-286.

Joglekar, A.P., K.S. Bloom, and E.D. Salmon. 2010. Mechanisms of force generation by end-on kinetochore-microtubule attachments. *Current opinion in cell biology*. 22:57-67.

Kelley, L.A., S. Mezulis, C.M. Yates, M.N. Wass, and M.J. Sternberg. 2015. The Phyre2 web portal for protein modeling, prediction and analysis. *Nat Protoc*. 10:845-858.

Khayrutdinov, B.I., W.J. Bae, Y.M. Yun, J.H. Lee, T. Tsuyama, J.J. Kim, E. Hwang, K.S. Ryu, H.K. Cheong, C. Cheong, J.S. Ko, T. Enomoto, P.A. Karplus, P. Guntert, S. Tada, Y.H. Jeon, and Y. Cho. 2009. Structure of the Cdt1 C-terminal domain: conservation of the winged helix fold in replication licensing factors. *Protein Sci*. 18:2252-2264.

Lee, C., B. Hong, J.M. Choi, Y. Kim, S. Watanabe, Y. Ishimi, T. Enomoto, S. Tada, Y. Kim, and Y. Cho. 2004. Structural basis for inhibition of the replication licensing factor Cdt1 by geminin. *Nature*. 430:913-917.

Maure, J.F., S. Komoto, Y. Oku, A. Mino, S. Pasqualato, K. Natsume, L. Clayton, A. Musacchio, and T.U. Tanaka. 2011. The Ndc80 loop region facilitates formation of kinetochore attachment to the dynamic microtubule plus end. *Current biology : CB*. 21:207-213.

Meraldi, P., R. Honda, and E.A. Nigg. 2004. Aurora kinases link chromosome segregation and cell division to cancer susceptibility. *Curr Opin Genet Dev*. 14:29-36.

Pozo, P.N., and J.G. Cook. 2016. Regulation and Function of Cdt1; A Key Factor in Cell Proliferation and Genome Stability. *Genes (Basel)*. 8.

Ramey, V.H., H.W. Wang, Y. Nakajima, A. Wong, J. Liu, D. Drubin, G. Barnes, and E. Nogales. 2011. The Dam1 ring binds to the E-hook of tubulin and diffuses along the microtubule. *Molecular biology of the cell*. 22:457-466.

Schmidt, J.C., H. Arthanari, A. Boeszoermenyi, N.M. Dashkevich, E.M. Wilson-Kubalek, N. Monnier, M. Markus, M. Oberer, R.A. Milligan, M. Bathe, G. Wagner, E.L. Grishchuk, and I.M. Cheeseman. 2012. The kinetochore-bound Ska1 complex tracks depolymerizing microtubules and binds to curved protofilaments. *Dev Cell*. 23:968-980.

Schmidt, J.C., and I.M. Cheeseman. 2011. Chromosome segregation: keeping kinetochores in the loop. *Current biology : CB*. 21:R110-112.

Spittle, C., S. Charrasse, C. Larroque, and L. Cassimeris. 2000. The interaction of TOGp with microtubules and tubulin. *The Journal of biological chemistry*. 275:20748-20753.

Tien, J.F., N.T. Umbreit, D.R. Gestaut, A.D. Franck, J. Cooper, L. Wordeman, T. Gonen, C.L. Asbury, and T.N. Davis. 2010. Cooperation of the Dam1 and Ndc80 kinetochore complexes enhances microtubule coupling and is regulated by aurora B. *The Journal of cell biology*. 189:713-723.

Umbreit, N.T., D.R. Gestaut, J.F. Tien, B.S. Vollmar, T. Gonen, C.L. Asbury, and T.N. Davis. 2012. The Ndc80 kinetochore complex directly modulates microtubule dynamics. *Proceedings of the National Academy of Sciences of the United States of America*. 109:16113-16118.

Varma, D., S. Chandrasekaran, L.J. Sundin, K.T. Reidy, X. Wan, D.A. Chasse, K.R. Nevis, J.G. DeLuca, E.D. Salmon, and J.G. Cook. 2012. Recruitment of the human Cdt1 replication licensing protein by the loop domain of Hec1 is required for stable kinetochore-microtubule attachment. *Nat Cell Biol*. 14:593-603.

Vavouri, T., J.I. Semple, R. Garcia-Verdugo, and B. Lehner. 2009. Intrinsic protein disorder and interaction promiscuity are widely associated with dosage sensitivity. *Cell*. 138:198-208.

Wang, H.W., S. Long, C. Ciferri, S. Westermann, D. Drubin, G. Barnes, and E. Nogales. 2008. Architecture and flexibility of the yeast Ndc80 kinetochore complex. *Journal of molecular biology*. 383:894-903.

Welburn, J.P., E.L. Grishchuk, C.B. Backer, E.M. Wilson-Kubalek, J.R. Yates, 3rd, and I.M. Cheeseman. 2009. The human kinetochore Ska1 complex facilitates microtubule depolymerization-coupled motility. *Developmental cell*. 16:374-385.

Welburn, J.P., M. Vleugel, D. Liu, J.R. Yates, 3rd, M.A. Lampson, T. Fukagawa, and I.M. Cheeseman. 2010. Aurora B phosphorylates spatially distinct targets to differentially regulate the kinetochore-microtubule interface. *Molecular cell*. 38:383-392.

Westhorpe, F.G., and A.F. Straight. 2013. Functions of the centromere and kinetochore in chromosome segregation. *Current opinion in cell biology*. 25:334-340.

Zaytsev, A.V., J.E. Mick, E. Maslennikov, B. Nikashin, J.G. DeLuca, and E.L. Grishchuk. 2015. Multisite phosphorylation of the NDC80 complex gradually tunes its microtubule-binding affinity. *Mol Biol Cell*. 26:1829-1844.

Zhang, G., C.D. Kelstrup, X.W. Hu, M.J. Kaas Hansen, M.R. Singleton, J.V. Olsen, and J. Nilsson. 2012. The Ndc80 internal loop is required for recruitment of the Ska complex to establish end-on microtubule attachment to kinetochores. *J Cell Sci*. 125:3243-3253.

Zhang, Q., S. Sivakumar, Y. Chen, H. Gao, L. Yang, Z. Yuan, H. Yu, and H. Liu. 2017. Ska3 Phosphorylated by Cdk1 Binds Ndc80 and Recruits Ska to Kinetochores to Promote Mitotic Progression. *Current biology : CB*.

Abbreviations: kMT, kinetochore-microtubule; MT(s), microtubule(s); Knl1, Kinetochore null 1; Ndc80, Nuclear division cycle 80; Mis12, Missegregation 12; CH, Calponin homology; MAP(s), Microtubule associated protein(s); Ska, Spindle and kinetochore-associated protein; TOG, Tumor overexpressed gene; MTBD, microtubule binding domain; WHD, Winged helix domain.

Figure Legends

Figure 1. Cdt1 is a novel microtubule-binding protein. (A) Disorder Prediction in human Cdt1. Disordered prediction (sum of 10 programs) is plotted as a function of residue number. (B) Seven homology models of full-length Cdt1; colored from N-terminus (blue) to C-terminus (red) with regions of low confidence or low overlap shown in translucent. Conserved WHM and WHC domains shown and aligned in grey and black,

respectively, for clarity. Magnified is the PyMol rendered cartoon representation showing superimposition of the C-terminal human Cdt1 (410-546 aa, in red) generated using Phyre2 server with available NMR structure (PDBid: 2KLO, in green) of mouse C-terminal Cdt1 (420-557 aa). (C) Constructs used in this study, full-length Cdt1 (546 aa), its deletion variant devoid of N-terminal 92 aa (92-546) and N- and C-terminal deletion variants generated in fusion with an N-terminal GFP tag for expression in bacteria are shown as black bars. Disordered domain shown in blue, winged helix middle (WHM) domain shown in yellow, and winged helix C-terminal (WHC) domain shown in red. (D) SDS-PAGE (15%) of the indicated purified recombinant proteins along with native tubulin purified from porcine brain. M, molecular mass standard. Asterisks (*) denote degradation bands (confirmed by western blot using Cdt1 antibody) in 92-410 fragment. Arrows point towards the band corresponding to the protein of interest. (E) Western blots showing MT co-sedimentation for the GFP-tagged human 92-546 and full-length 1-546 Cdt1 (without any tag), 1 μM each; purified from bacteria with the indicated concentrations of taxol-stabilized MTs (in μM). Samples fractionated as Supernatant (S) and Pellet (P) were analyzed by western blot probed with antibodies against 6×-His tag or anti-Cdt1 as indicated in each case to detect Cdt1. Ponceau S stained tubulin. (F) Quantification (Mean ± SD, n=3) of the 92-546 and 1-546 Cdt1 blots using Image J. The 95% CI values obtained for the fit were 0.60-0.94 for B_{max}, 0.37-4.04 for K_d and 0.07-0.29 for the background for the former and xxxxxx for the latter. (G) Representative western blots of the binding of indicated deletion fragments to MTs in a co-sedimentation assay with the indicated MT concentrations (top). (H) Quantification of binding (Mean ± SD, n=3) of the deletion

fragments to MTs. (I) Quantification of MT-binding of Cdt1 C-terminal fragment, GFP-410-546 and a representative western blot (top).

Figure 2. Cdt1 diffuses on MTs *in vitro* and decorate spindle microtubules *in vivo*. (A) Representative western blot of 92-546 Cdt1 (1 μM) co-sedimentation with intact (MT) or subtilisin-treated (ST-MT) microtubules at 1 and 4 μM concentrations. (B) Quantification of (A). (C) Quantification of co-sedimentation of 92-546 Cdt1 (1 μM) with 16 μM MTs in the absence (+MT) and presence of 250 mM NaCl (+MT+S) (top). Representative western blot shown (bottom). (D) Single channel and merged TIR-FM images showing surface immobilized Dylight405-labeled MTs (blue) and GFP-tagged 92-546 Cdt1 (green). (E) Kymograph analysis of GFP-tagged 92-546 interactions with the MT lattice. (F) Cumulative frequency plot and exponential fit of 92-546 dwell times. N=304 molecules, 2 independent protein preparations. (G) Diffusion coefficient analysis of 92-546 Cdt1 on MTs carried out using DiaTrack particle tracking Software. Inset graph shows the histogram distribution of number of particles of 92-546 Cdt1 that diffused on MTs within the range of 0-1 $\mu m^2/s$. (H) The un-transfected mitotic HeLa cell stained with anti-Cdt1 and either anti-tubulin antibody (H, top panels) or anti-Hec1 antibody (H, bottom panels). Scale bar, 5 μm. (I) and (J) Immunostaining of transiently transfected or stably transfected HeLa cells with anti-HA and anti-tubulin antibodies; DNA stained is blue with DAPI in the panels indicated. (K) Insets from the image stack of the mitotic cell in the top panels of J (left) with an example from another cell (not depicted). The panels, H-K depict confocal images of cells in metaphase, interphase and cytokinesis. (I) Western blot of

mock and transfected lysates probed with antibodies against human Cdt1 (using anti-HA or anti-Cdt1) and mouse tubulin as loading control.

Figure 3. Aurora B Kinase (ABK) targets Cdt1 for phosphorylation *in vitro* and affects Cdt1-MT binding. (A) Sequence alignment of Cdt1 from the indicated species using Clustal Omega. Highlighted in the red font are the potential Ser/Thr ABK sites. On the top, mentioned are the residues and their positions with respect to the full-length human Cdt1 (1-546 aa). (B) *In vitro* kinase assay with ABK alone or ABK plus ZM447439 inhibitor (10 µM) on HEK 293-purified Cdt1 or hVimentin (as a positive control). The autoradiogram (top) and Coomassie-stained gel (bottom) are shown. "M" denotes migration of molecular mass standards in kDa on a 12 % SDS-PAG. (C) Co-immunoprecipitation of ABK by HA/His-tagged Cdt1-WT or Cdt1-T29A Cdk1-mutant from thymidine synchronized and nocodazole arrested mitotic HeLa cell extracts. The IP was performed using Ni^{+2}-NTA agarose beads followed by immunoblotting with both anti-HA or anti-ABK antibodies. 1% of the lysate was loaded as input. HEK-cells expressing GFP were used as a control. (D) Schematic representation showing the full-length Cdt1 (546 aa) and its deletion variant devoid of N-terminal 92 aa generated in fusion with GFP tag for expression in bacteria. The following two proteins generated represent ABK phosphomimetic (8D, Ser/Thr substituted with Asp) and phospho-deficient (8A, Ser/Thr substituted with Ala) Cdt1 mutants. (E) Quantification (Mean ± SD, n = 3) showing MT co-sedimentation of purified 92-546 Cdt1 or the mutant proteins (1 µM each) with the indicated concentrations of taxol-stabilized MTs (in µM). The 95% CI values obtained for each fit were: B_{max}=0.34-0.65, K_d=0.43-10.57 for 8D and B_{max}=0.36-0.67, K_d=0-3.22 for

8A. (F) Representative western blot is shown. Samples fractionated as Supernatant (S) and Pellet (P) analyzed by Western blot probed with antibody against 6×-His tag to detect Cdt1 and stained with Ponceau S for tubulin.

Figure 4. Aurora B phosphorylation of Cdt1 regulates kinetochore microtubule stability and mitotic progression. (A) Synchronized HeLa cells treated with siRNA against endogenous Cdt1 in G2/M phase and rescued with stably expressing siRNA-resistant Cdt1-WT or 10D (phosphomimetic) and 10A (unphosphorylated) proteins were stained with antibodies against Zwint-1 in red (1:500 dilution, kinetochore/centromere marker), MTs in green (1:500 dilution, spindle marker) and DAPI in b/w marking the nucleus. Cells were placed at 4°C for 15 min before being fixed and stained. (B) A bar graph showing the quantification of MT staining intensity in each case after background subtraction (n = 10 cells). (C) Quantification of the % of bi-attached, bi-oriented kinetochores along with a cropped image of representative kinetochore pairs in each of the conditions as indicated. Kinetochore marker, Zwint1, is in red and MTs is in green. (D) Inter-kinetochore (K-K) stretch was calculated between the two kinetochore pairs in each case and is plotted (*n*=115 pairs; 10 cells). (E) Mitotic progression (metaphase to anaphase transition) was assessed in HeLa cells stably expressing vector, Cdt1-WT, ABK Cdt1-phosphomimetic (10D) or phospho-defective (10A) mutants at 11.5 and 12.5 h after release from thymidine treatment. DAPI in red stains the nucleus and antibody against tubulin stained the MTs green. (F) The number of cells in each stage of mitosis were counted and plotted from three different coverslips of two independent experiments to illustrate the nature of mitotic delay/arrest in Cdt1-10D mutant-expressing cells as

compared to cells rescued with Cdt1-WT or Cdt1-10A expression (n = 600 cells; a and b represent the statistical significance obtained using non-parametric students *t* test performed on the WT *vs* 10D in the indicated stages of mitosis).

Figure 5: A Model depicting the role of Cdt1 in providing an additional kMT-attachment site besides the CH and the N-terminal tail domain of the Ndc80 complex. (A) Comparative tabulation of MT-binding parameters and phospho-regulation of relevant kinetochore associated proteins from vertebrates. (B) The calponin homology (CH) domains in Hec1 and Nuf2 along with the Hec1 unstructured tail bind MTs. The unstructured ~40 aa loop region of Hec1 recruits Cdt1 by interacting with the N-terminal 1-320 aa of Cdt1 (Varma et al., 2012). This induces a conformational shift in the Ndc80 complex in a manner that is dependent on Cdt1 binding to MTs. In prometaphase when kinetochores are not bi-oriented, ABK is active to destabilize the erroneous attachments by phosphorylating several kinetochore proteins including Ndc80 (1), Ska (2), and Cdt1 (3) shown in the present study, all of which bind to MTs. Upon phosphorylation, these proteins exhibit reduced affinity for MTs. As observed for the Ska complex which cannot interact with the KMN network effectively upon its phosphorylation by ABK (4); whether Cdt1~P can dock on to the Hec1 loop (5) with similar efficiency as unphosphorylated Cdt1 is still undetermined. In metaphase, when the ABK gradient diminishes at kinetochores, Cdt1 becomes proficient to binds to MTs (6), thus providing an additional site for kMT attachment besides the CH and the tail domains of Ndc80. Whether Cdt1 can interact with the Ska complex in its free or loop-bound state and if this interaction is dependent on their phosphorylation status (7 and 8) is yet to be determined. The model also depicts

the possibility of interaction of other MAPs with the Hec1 loop either alone or with the help of Cdt1 or Ska or both (9), as shown using dashed arrows.

Materials and methods

Chemicals, reagents, cell lines and bacterial strains

Bacterial strains for cloning and expression were grown in Luria-Bertani (LB) broth or agar supplemented with 100 µg/ml ampicillin or 50 µg/ml kanamycin as appropriate. Enzymes for cloning were purchased from New England Biolabs (Beverly, MA). Custom oligonucleotides and G-blocks were from Integrated DNA Technologies (Coralville, IA). Sanger DNA sequencing was conducted at the Northwestern University Genomics core facility.

DNA manipulations: cloning and mutagenesis

Cdt1 gene sequence was codon optimized and was synthesized as a linear DNA strand (G-block, IDT) for subsequent cloning procedures. The largest Cdt1 fragment (92-546 aa), deletion variants (92-232 aa, 92-410 aa, 410-546 aa) and Aurora B phosphomimetic mutants (Ser101Asp, Thr102Asp, Ser143Asp, Ser265Asp; Thr270Asp, Thr287Asp, Thr329Asp, Thr358Asp abbreviated as 8D) and non-phosphorylatable mutants (Ser101Ala, Thr102Ala, Ser143Ala, Ser265Ala; Thr270Ala, Thr287Ala, Thr329Ala, Thr358Ala abbreviated as 8A); were cloned in fusion with the N-terminal GFP and 6×-His tags using SspI and Gibson cloning in a commercial plasmid procured from Adgene (pET His6 GFP TEV LIC cloning vector (1GFP), plasmid #29663).

For stable transfections, the genes encoding Cdt1 with mutations that represent Aurora B phosphomimetic (Thr7Asp, Ser73Asp, Ser101Asp, Thr102Asp, Ser143Asp, Ser265Asp; Thr270Asp, Thr287Asp, Thr329Asp, Thr358Asp) and non-phosphorylatable (Thr7Ala, Ser73Ala, Ser101Ala, Thr102Ala, Ser143Ala, Ser265Ala; Thr270Ala, Thr287Ala, Thr329Ala, Thr358Ala) versions, abbreviated as 10D and 10A, respectively harboring C-terminal 2×-HA, Strep-tag, 12×-His tag were cloned in pQCXIP plasmid using custom gene synthesis services (Thermofisher Scientific).

In silico analyses

Secondary Structure Prediction

The protocol was based on the work of Seeger *et al*. (Seeger et al., 2012). The full sequence of human Cdt1 (Uniprot ID: Q9H211) was input into ten different secondary structure prediction servers to reduce the bias from any one program. The prediction of disordered regions is based on amino acid composition, charge/hydropathy index, known disordered sequences from crystal/NMR structures, and other empirical methods. The servers included were PSIPRED, IUPRED, PONDR, FoldIndex, s2D, ESpritz, PROFsec, MFD2p, DISCoP, and YASPIN. Relatively stringent cutoff of >75% within each algorithm was used to classify a residue as “disordered.” The results of each server were converted to a binary output of “folded/unknown” or “disordered” (0 or 1 respectively). The scores were summed and plotted as a function of amino acid number.

Homology Modeling

The full sequence of human Cdt1 (Uniprot ID: Q9H211) was input into the Phyre2 (Kelley et al., 2015), I-TASSER (Roy et al., 2010), and SWISS-MODEL (Schwede et al., 2003)

homology modeling servers. Models were aligned using the “cealign” plugin on Pymol. The C-terminal winged helix domain was chosen to align all models. Crystal structures from human WHM domain (PDB ID:2WVR) (De Marco et al., 2009) and mouse WHC domain (PDB: 2KLO) (Khayrutdinov et al., 2009) were used as templates for the winged helix domains. Pymol was used to generate protein structure images and the final figures were generated in Adobe Illustrator.

Recombinant Protein Expression and Purification

For MT co-pelleting assays, the fusion proteins along with the GFP protein (as a control) were purified from the soluble fraction after over-expression in BL21(λDE3) at 23 ºC for 18 h in LB medium, using nickel-affinity chromatography. The proteins purified to 85% purity were dialyzed in 20 mM Tris-HCl, pH 8.0 with 300 mM NaCl and stored in -20 ºC until further use. Full length Cdt1 (1-546 aa) was purified as a GST tagged protein using pGEX-5X-1 followed by tag removal as described previously.

Native tubulin was purified from porcine brains as previously described (Williams and Lee, 1982), flash frozen, stored in aliquots in liquid nitrogen, and clarified of aggregates by centrifugation at 100,000 × *g* prior to use.

Full-length human Cdt1 (1-546 aa) purified from HEK293 cells with a C-terminal Myc/DDK tag dialyzed in 25 mM Tris-HCl, pH 7.3, 100 mM glycine and 10% glycerol was purchased from Origene (TP301657).

For TIRF assays, human Cdt1 (GFP tagged-Δ92-546) was induced in BL21(λDE3) cells at 30 ºC for 5 h in enriched terrific broth. Cells pellets were flash frozen in liquid nitrogen and stored at -80 ºC. Cell pastes were lysed via sonication, and spun at 35,000

rpm for 45 min. The soluble fraction was incubated with 6 mL of 50% cobalt IMAC resin (TALON, Clontech) for 1 h at 4 ºC. The beads were washed with 100 mL of wash buffer (25 mM HEPES pH 7.4, 500 mM NaCl, 2.5 mM imidazole, 5% sucrose w/v and 0.5 mM TCEP) and eluted with 15 mL of elution buffer (wash buffer + 500 mM imidazole). The eluted protein was concentrated to approximately 2.5 mL and injected over a Superdex 200 16/60 SEC column (GE Healthcare) in storage buffer (25mM HEPES pH 7.4, 500 mM NaCl, 0.5 mM TCEP, 5% sucrose w/v). Purified, folded Cdt1 eluted at approximately 65 mL and was monodisperse. The final protein was ~95% pure via SDS-PAGE. Protein was flash frozen in liquid nitrogen and stored at -80 ºC until use.

Microtubule co-pelleting assay

For microtubule-binding assay, tubulin was polymerized and stabilized in general tubulin (GT) buffer, BRB80 (80 mM PIPES pH 6.8, 1 mM $MgCl_2$, 1 mM EGTA) with 100 mM GTP, 20 µM Paclitaxel/taxol and 66 % glycerol (assay buffer). The proteins (diluted in BRB80 buffer containing 1 mg/ml BSA) were pre-cleared of any aggregates or debris by ultracentrifugation at 70,000 rpm at room temperature for 30 min. The taxol-stabilized MTs (in varying micromolar concentrations) were incubated with indicated concentration of pre-cleared protein(s) or 2 µM of GFP/GST alone to a final reaction volume of 40 µl. Reactions were incubated at room temperature for 20 min and ultra-centrifuged for 30 min at 60,000 rpm in a Beckman TLA100 rotor at 25 °C. The binding was also carried out in the presence of salt by adding 300 mM NaCl to the assay buffer. Pellets (P) and supernatants (S) were separated carefully, equal volumes of SDS sample buffer was added and then samples were run on SDS-PAG and analyzed by Western blotting with

anti-His Monoclonal antibody (1:5000, Abcam) or Cdt1 polyclonal IgG raised in rabbit (1:2000, H-300, sc-28262, Santa Cruz Biotech). Immunoblots were scanned onto Adobe Photoshop and any manipulations to the brightness were applied to the entire image. Densitometry quantification of the bands representing the arbitrary amount of protein in supernatants and pellets was done using ImageJ software (National Institutes of Health, Bethesda, MD). The percentage binding was measured by calculating the ratio of protein in the pellet (P) and the total protein (S+P). The fraction of protein bound was then plotted against the concentration of MTs, and the data were fit to the single-site saturation non-linear regression curve (with no non-specific binding but background and K_d>0 constrain) using GraphPad Prism 6.0 (San Diego, CA). The K_d values generated represent the average and propagated error from at least three independent experiments.

For co-sedimentation assays with subtilisin-treated microtubules, 20 μM taxol-stabilized microtubules were incubated for 30 min at 30°C with 200 μg/ml subtilisin A (Calbiochem), a serine protease that cleaves the C-terminal 10–20 amino acids from α- and β-tubulin. The reaction was stopped with 10 mM PMSF, digested MTs were pelleted (90,000 rpm, TLA100, 10 min, 25 °C) and resuspended in the original volume of GT buffer. The assay was then carried out as described above.

Curved tubulin oligomers or rings were generated by incubating tubulin with Dolastatin (Tocris Bioscience) dissolved in dimethyl sulfoxide (DMSO) in a 2:1 molar ratio for 1 h at room temperature in GT buffer supplemented with 6% DMSO. The rings were purified by ultracentrifugation through a cushion of GT buffer with 40 % glycerol. The rings were resuspended in the original volume of GT buffer and assay was carried out as described before. Sheared microtubules were prepared by passing taxol-stabilized

microtubules through a $26_{1/2}$-gauge needle multiple times immediately before the addition to the protein sample. The generation of increased number of ends was confirmed by transmission electron microscopy (TEM).

Total internal reflection fluorescence microscopy (TIR-FM)

Flow chambers containing immobilized MTs were assembled as described (McKenney et al., 2014). Imaging was performed on a Nikon Eclipse Ti-E microscope equipped with an Andor iXon EM CCD camera; a 100×, 1.49 NA objective and 1.5x tube lens (yielding a pixel size of 106 nm); four laser lines (405, 491, 568, and 647 nm); and using the Micro-Manager software (Edelstein et al., 2014). All assays were performed in assay buffer (30 mM Hepes [pH 7.4], 50 nM K-acetate, 2 mM Mg-acetate, 1 mM EGTA, and 10% glycerol), supplemented with 0.1 mg/mL biotin-BSA, 0.5% Pluronic F-168, and 0.2 mg/mL κ–casein. A final concentration of 1 and 5 nM GFP-tagged Δ92-546 human Cdt1 was used. Protein samples from two independent purification batches were used to ensure biological reproducibility. Photobleaching tests (Helenius et al., 2006) revealed the photobleaching rate of this construct under our conditions exceeded the characteristic dwell time by approximately three-fold and thus our dwell time calculations do not take photobleaching into account. Dwell times were calculated manually from kymographs of individual MTs and plotted in GraphPad Prism 7.0.

For measuring the diffusion coefficient, the TIR-FM imaging time series of GFP-Cdt1 were first bleach-corrected by histogram matching using Image J Software and saved as 8-bit multi-page TIFF files before being transferred to the DiaTrack 3.04 Pro particle tracking Software (http://www.diatrack.org/), which was then used to identify and

track GFP particles localized on microtubules. The read-out for diffusion coefficient obtained from the tracking Software was in $(pixel)^2$/sec and the time interval between individual time frames of the TIR-FM time series was ~65 milliseconds. Thus, each read-out in $(pixel)^2$/sec was first multiplied by the pixel size in µm (0.106 µm), and again by a factor of ~15.4 (milliseconds to seconds conversion) to obtain final values in $(\mu m)^2$/sec. The particles that showed high diffusion were excluded for the calculation of the diffusion coefficient (D), along with the stationary particles. This was done because in the time frame used to conduct the analysis, we were unable to ascertain with accuracy whether these particles were indeed bound to and diffusing along MTs.

In vitro phosphorylation assay

In vitro kinase assay was performed on 1 µg each of hekCdt1 and human Vimentin (ab73843, Abcam) at 30°C for 1 h in assay buffer containing 25 mM Hepes, 50 mM NaCl, 1 mM DTT, 2 mM EGTA, 5 mM $MgSO_4$, 10 µM ATP, 5 µCi γ-[^{32}P] ATP (Perkin Elmer) in the presence of 0.5 µg Aurora B Kinase (AURKB-231H, Creative BioMart) alone or with its inhibitor ZM447439 (10 µM, obtained from Sigma). Samples (30 µl) were then electrophoresed on SDS-PAG and visualized by autoradiography. The same gel was stained with coomassie to ascertain migration of the proteins.

Sample preparation for Mass spectroscopy, LC-MS/MS and Data analysis

Both non-radioactive kinased and control samples were precipitated overnight at -20ºC with 8 volumes of acetone and 1 volume of TCA. The protein was pelleted by centrifugation at 15,000 × g for 15 min at 4ºC. The pellets were washed twice with 200 µL

cold acetone, dried and re-suspended in 8 M urea/0.4 M ammonium bicarbonate, then reduced with 4 mM DTT for 30 min at 50ºC. Alkylation with 18 mM iodoacetamide was carried out at room temperature for 30 min in dark. The urea was diluted to less than 2 M with ultrapure water followed by addition of sequencing-grade trypsin (Promega) for overnight in a ratio of 1:18 (enzyme: substrate). The peptides were desalted using C18 spin columns according to the manufacturer's instructions. Samples were re-suspended in 5 % acetonitrile (ACN) /0.1 % formic acid (FA) to a final concentration of 0.15ug/μL.

Nano LC-MS/MS analyses were performed with a 75 µm x 10.5 cm PicoChip column packed with 3 µm Reprosil C18 beads. A 150 µm x 3 cm trap packed with 3um beads was installed in-line. Solvent A consisted of 0.1 % FA in water and solvent B was 0.1 % in ACN. Peptides were trapped at 5 µL/min for 5 min, then separated at a flow rate of 300 nL/min with a gradient from 5 % to 30 % B in 95 min. After a 5 min ramp to 60 % B, the column was washed at 95 % B and re-equilibrated to 5 % B with a total analysis time of 120 min. Desalted phosphopeptide-enriched fractions were re-suspended in 5 % ACN/0.1 % FA. Six microliters (0.9 μg) were injected in duplicates for each sample.

The LC was coupled by electrospray to a Q-Exactive HF mass spectrometer operating in data-dependent MS/MS mode with a top-15 method. Dynamic exclusion was set to 60 s and charge 1+ ions were excluded as well. MS^1 scans were collected from 300-2000 *m/z* with resolving power equal to 60,000 at 400 *m/z*. The MS^1 AGC was set to 3×10^6. Precursors were isolated with a 2.0 m/z isolation width, and the HCD normalized collision energy was set to 35%. The MS^2 AGC was set to $1x10^5$ with a maximum ion accumulation time of 120ms, and the resolving power was 30,000.

MS raw files were searched against the human SwissProt database (version downloaded 8/2016, 20191 sequences) using the Mascot search engine. Cysteine carbamidomethylation was a fixed modification and the variable modifications were oxidized methionine, acetylation of protein N-terminus, deamidation of Asn/Gln, and phosphorylation of Ser, Thr, and Tyr residues. Two missed cleavages were allowed. Statistical cutoffs and data visualization were accomplished using Scaffold Q+ software (Proteome Sciences). Proteins were selected with a 1 % FDR cutoff and peptides with a 90 % identification probability or better were considered. All phosphopeptide spectra were inspected manually to determine whether the phosphate group had been assigned to the correct amino acid.

Cell culture methods

Transient or stable transfections, immunofluorescence and confocal microscopy

HeLa or HEK 293 FT cells were cultured at 37°C with 5 % CO_2 in Dulbecco's modified eagle's medium (DMEM, Life Technologies) containing 10 % fetal bovine serum (Seradigm, VWR Life Science), 100 U ml^{-1} penicillin and 1 µg ml^{-1}streptomycin.

Prior to transfection, cells were seeded overnight onto 18 mm circular coverslips to achieve ~ 60-70 % confluency. The cells were then transfected with 0.5 µg of pJC13-Cdt1-HASH plasmid (carrying C-terminal tags: 2× HA, Strep-tag, 12× His tag followed by a stop codon; a generous gift from Jeanette Cook at the UNC) using Effectene transfection reagent (Qiagen) according to the manufacturer's protocol. After 36 h, the cells were fixed in phosphate buffer saline (pH 7.2) containing 4 % formaldehyde followed by staining with antibody against the HA tag (1:100, H6908, Sigma), Tubulin monoclonal

antibody (1:500, T9026, clone DM1A Sigma) and 4,6-diamino-2-phenylindole (DAPI) dihydrochloride (1:10,000, Life Technologies). Alexa Fluor 488-, Rhodamine Red-X-, or Cy5-labeled donkey secondary antibodies used at 1:250 dilution each were obtained from Jackson ImmunoResearch Laboratories, Inc.

To generate stable cell lines, pQCXIP, a bicistronic retroviral expression vector was used (Julius et al., 2000). Upon transfection into HEK-293T packaging cell line, this vector integrates and stably expresses a viral genomic transcript containing the CMV immediate early promoter, gene of interest, IRES and the puromycin resistance gene (Pur^R). The gene of interest and the puromycin resistance gene are co-transcribed, via the internal ribosome entry site (IRES), as a bicistronic message (Adam et al., 1991; Goshima and Yanagida, 2000). HEK-293T cells were seeded at a density of 0.75×10^6 in 10-cm dish. A three plasmid transfection system containing carrier pQCXIP plasmid (5 µg) expressing the gene of interest (*cdt1*-WT or 10D or 10A) along with the two helper plasmids pVSV-G, 1.25 µg (Clonetech) and pCL-eco, 3.75 µg (Imagenex) encoding the Env and Gag/Pol proteins required for virus production was used. The HEK cells were transfected using calcium phosphate for 48 h and the culture supernatant containing viral particles was harvested and passed through 0.45 µm syringe filter. Fresh media was added to the dish for second round of collection at 72 h. Next, polybrene (8 µg/ml) was mixed with the filtered virus followed by addition of the virus on to the target HeLa cells (seeded at a density of 6.5×10^4 in a 10-cm dish) for 6 h. Selection for the stably integrated cells was performed for 2 weeks by addition of 1 µg/ml puromycin, a concentration determined to kill 100 % of control un-transduced HeLa cells.

For image acquisition, the coverslips were mounted using ProLong® Gold Antifade reagent (Invitrogen), 3D stacks were obtained sequentially at 200-nm steps along the z axis through the cell using a high-resolution inverted microscope (Eclipse TiE; Nikon) equipped with a spinning disk (CSU-X1; Yokogawa Corporation of America), an Andor iXon Ultra888 EMCCD camera, and an x60 or x100 1.4 NA Plan-Apochromatic DIC oil immersion objective (Nikon). The images were acquired and processed using the NIS elements Software from Nikon.

siRNA transfections, double thymidine synchronization and cold stability assay

HeLa cells were synchronized by treatment with 2 mM thymidine for 18 h followed by release for 9 h and then re-treatment with 2 mM thymidine for 18 h. Synthetic duplexed RNA oligonucleotide (siRNA) against Cdt1 was transfected into HeLa cells according to the manufacturer's instructions as described previously (Varma et al., 2012) during the 2nd thymidine release and prior to fixing the cells at designated time points as indicated in figure 4 and associated legends. Other cell manipulations include cold treatment for 15 min with ice-cold PBS prior to fixation.

Co-immunoprecipitation

HEK-293T cells were transfected with the plasmids (Cdt1-HASH or T29A mutant in pQCXIP and pEGFP-N1) for 4 h at 20-30% confluency using PEI max transfection reagent. M phase synchronization was done by treating the cells with 2 mM thymidine for 18 h, followed by addition of 100 ng/ml (0.33 μM) Nocodazole for 10 h. The cells were collected by mitotic-shake-off and lysed using lysis buffer (50 mM HEPES pH 8.0, 33 mM KAc, 117 mM NaCl, 20 mM Imidazole, 0.1% triton, 10% glycerol, 0.1 mM AEBSF, 10

μg/ml pepstatin A, 10 μg/ml aprotinin, 10 μg/ml leupeptin, 1 mM ATP, 1 mM $MgCl_2$, 5 μg/ml phosvitin, 1 mM β-glycerol-phosphate, 1 mM orthovanadate). The whole cell lysates expressing the His-tagged proteins were incubated with Ni^{+2}-NTA beads for 3 h with end-on rotation at 4°C. Beads were washed three times with the lysis buffer, and bound proteins were eluted by boiling for 5 min in 40 μL of 2× SDS sample buffer. For immunoblotting, proteins were electrophoresed on SDS-PAG and transferred to the PVDF membranes. Immunoblots were developed using chemiluminescence and exposed on to the X-ray films. Antibodies against Aurora B Kinase and HA-tag were procured from Abcam (ab2254) and Sigma (H6908), respectively.

Figure 1

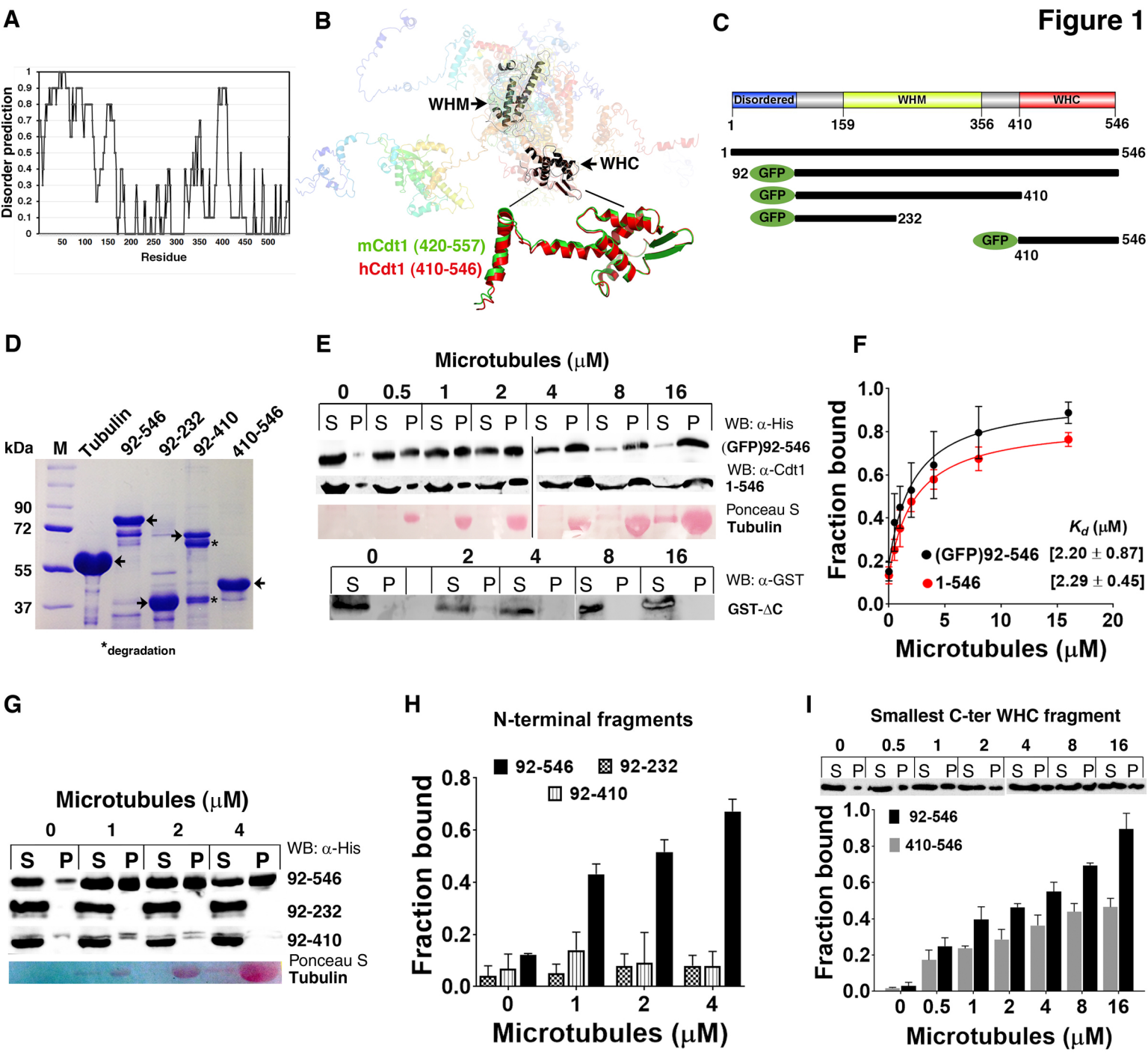
A
Disorder prediction
Residue
B
WHM
WHC
mCdt1 (420-557)
hCdt1 (410-546)
C
Disordered
WHM
WHC
1
159
356
410
546
92
GFP
232
D
kDa
M
Tubulin
92-546
92-232
92-410
410-546
90
72
55
37
*degradation
E
Microtubules (μM)
0
0.5
1
2
4
8
16
S
P
WB: α-His
(GFP)92-546
WB: α-Cdt1
1-546
Ponceau S
Tubulin
WB: α-GST
GST-ΔC
F
Fraction bound
Microtubules (μM)
K_d (μM)
(GFP)92-546 [2.20 ± 0.87]
1-546 [2.29 ± 0.45]
G
Microtubules (μM)
WB: α-His
92-546
92-232
92-410
Ponceau S
Tubulin
H
N-terminal fragments
92-546
92-232
92-410
Fraction bound
Microtubules (μM)
I
Smallest C-ter WHC fragment
92-546
410-546
Fraction bound
Microtubules (μM)

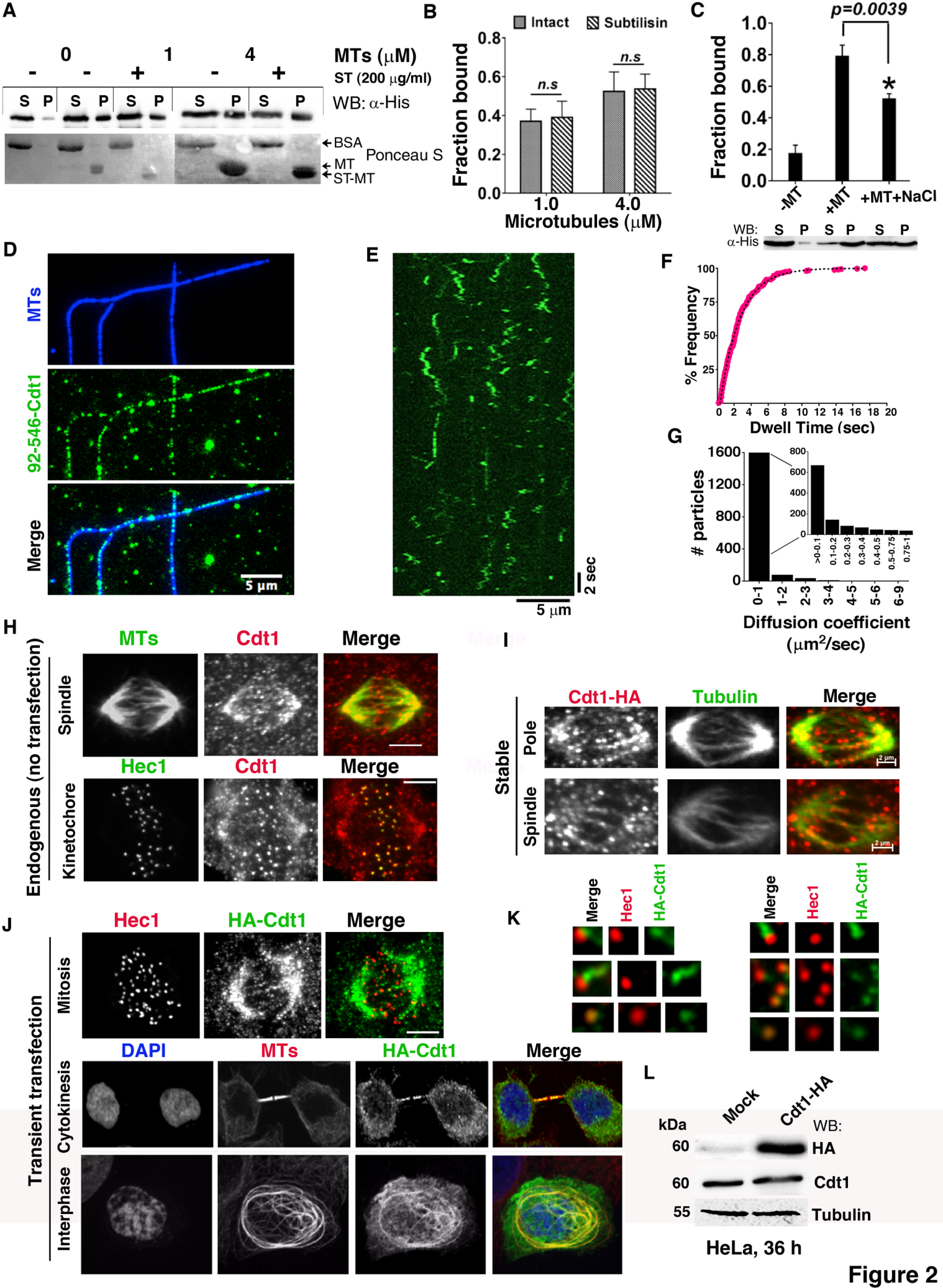
A
0
1
4
MTs (μM)
ST (200 μg/ml)
S P S P S P S P S P
WB: α-His
BSA
MT
ST-MT
Ponceau S
B
Intact
Subtilisin
Fraction bound
n.s
n.s
1.0
4.0
Microtubules (μM)
C
p=0.0039
Fraction bound
-MT
+MT
+MT+NaCl
WB: α-His
S P S P S P
D
MTs
92-546-Cdt1
Merge
5 μm
E
2 sec
5 μm
F
% Frequency
Dwell Time (sec)
G
particles
Diffusion coefficient (μm²/sec)
H
MTs
Cdt1
Merge
Spindle
Hec1
Cdt1
Merge
Kinetochore
Endogenous (no transfection)
I
Cdt1-HA
Tubulin
Merge
Stable
Pole
Spindle
J
Hec1
HA-Cdt1
Merge
Mitosis
DAPI
MTs
HA-Cdt1
Merge
Cytokinesis
Interphase
Transient transfection
K
Merge
Hec1
HA-Cdt1
L
Mock
Cdt1-HA
kDa
WB:
60
HA
60
Cdt1
55
Tubulin
HeLa, 36 h

Figure 2

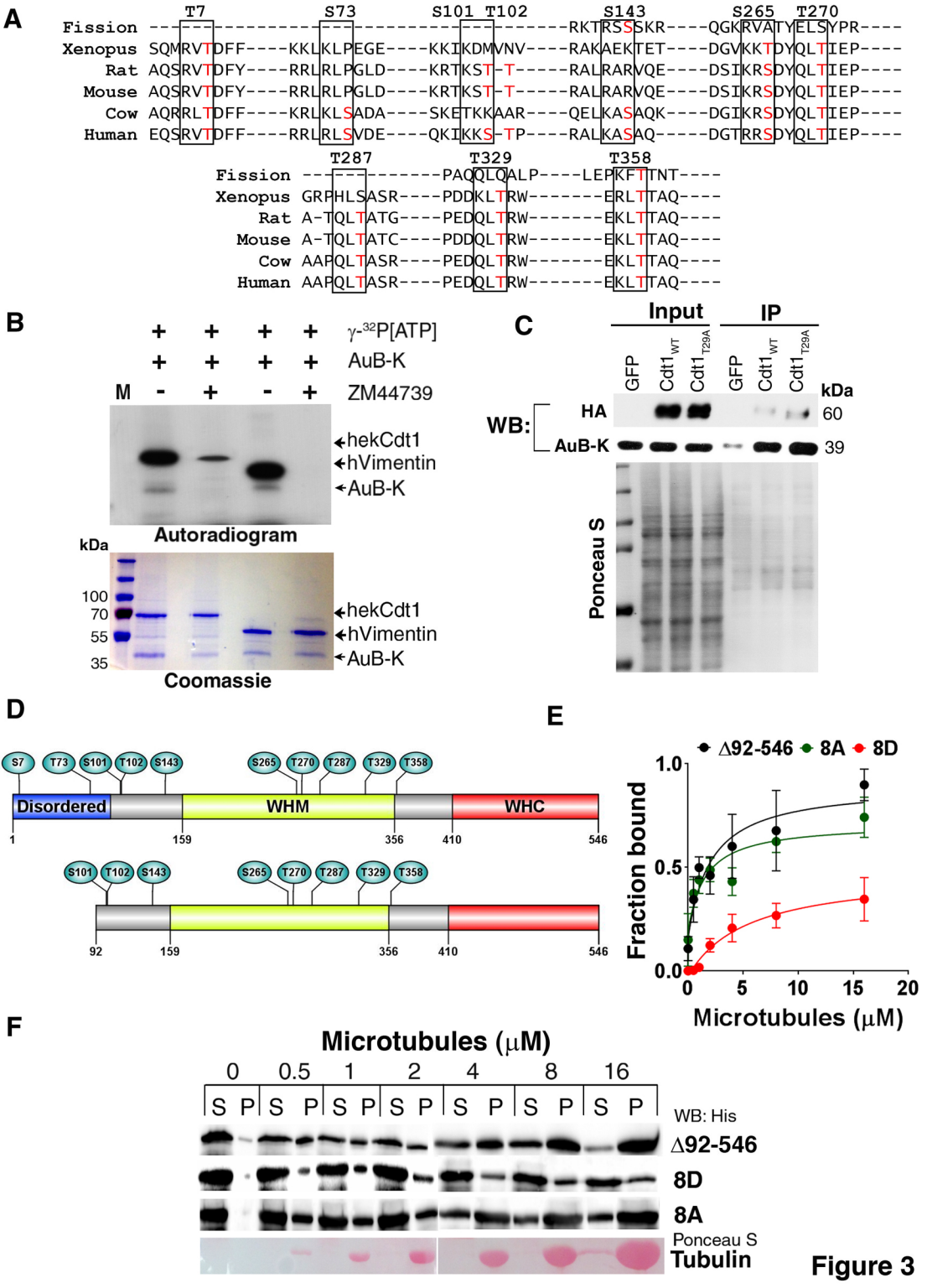
A
T7 S73 S101 T102 S143 S265 T270
Fission
Xenopus
Rat
Mouse
Cow
Human
T287 T329 T358
B
γ-32P[ATP]
AuB-K
M
ZM44739
hekCdt1
hVimentin
AuB-K
Autoradiogram
kDa
100
70
55
35
Coomassie
C
Input
IP
GFP
Cdt1WT
Cdt1T29A
kDa
WB:
HA
AuB-K
60
39
Ponceau S
D
S7
T73
S101
T102
S143
S265
T270
T287
T329
T358
Disordered
WHM
WHC
1
159
356
410
546
92
E
Δ92-546
8A
8D
Fraction bound
1.0
0.5
0.0
0
5
10
15
20
Microtubules (μM)
F
Microtubules (μM)
0
0.5
1
2
4
8
16
S P
WB: His
Δ92-546
8D
8A
Ponceau S
Tubulin

Figure 3

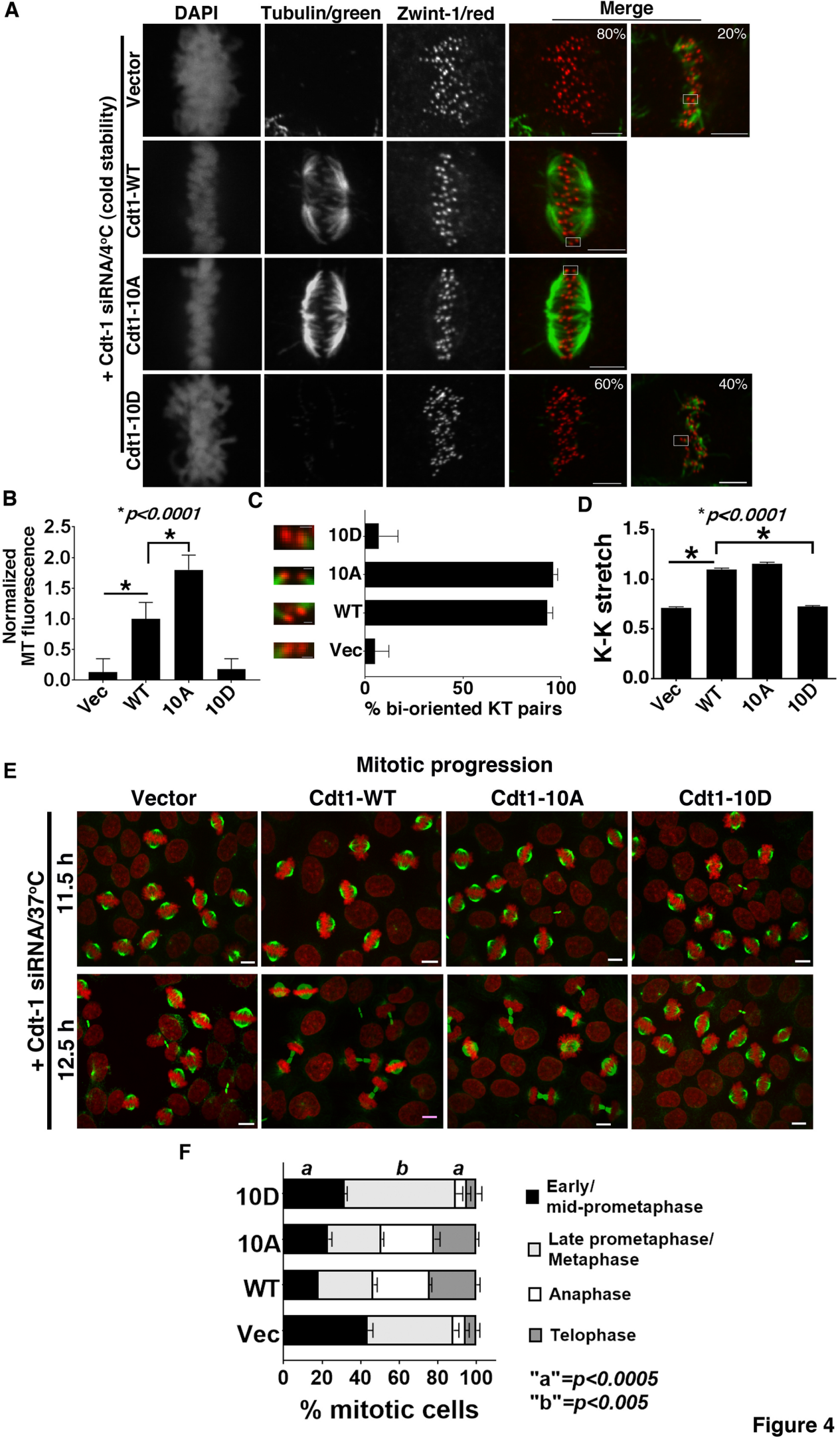
A
DAPI
Tubulin/green
Zwint-1/red
Merge
80%
20%
60%
40%
+ Cdt-1 siRNA/4°C (cold stability)
Vector
Cdt1-WT
Cdt1-10A
Cdt1-10D
B
*p<0.0001
Normalized MT fluorescence
2.5
2.0
1.5
1.0
0.5
0.0
Vec
WT
10A
10D
C
10D
10A
WT
Vec
0
50
100
% bi-oriented KT pairs
D
*p<0.0001
K-K stretch
1.5
1.0
0.5
0.0
Vec
WT
10A
10D
E
Mitotic progression
Vector
Cdt1-WT
Cdt1-10A
Cdt1-10D
+ Cdt-1 siRNA/37°C
11.5 h
12.5 h
F
a
b
a
10D
10A
WT
Vec
0
20
40
60
80
100
% mitotic cells
Early/ mid-prometaphase
Late prometaphase/ Metaphase
Anaphase
Telophase
"a"=p<0.0005
"b"=p<0.005

Figure 4

A

	hNdc80	hSka	hCdt1
MT binding	+	+	+
K_d (μm)	Variable	2.5	2.2
Diffusion ($\mu m^2/s$)	$0.03_{Broccoli}$ 0.078_{Bonsai}	0.18	0.16
ΔE-hooks	Reduced	Unaffected	Unaffected
Motif/domain	CH/tail	WTH	WHM/C?
Region	N-ter.	C-ter./132-255 aa	C-ter./central?
MT-type	Straight	Straight/curved	Straight/curved
Kinase	ABK	ABK, Cdk1, Mps1*	ABK, MAPK?, Cdk1? Mps1?

*Maciejowski *et al.*, 2017

B

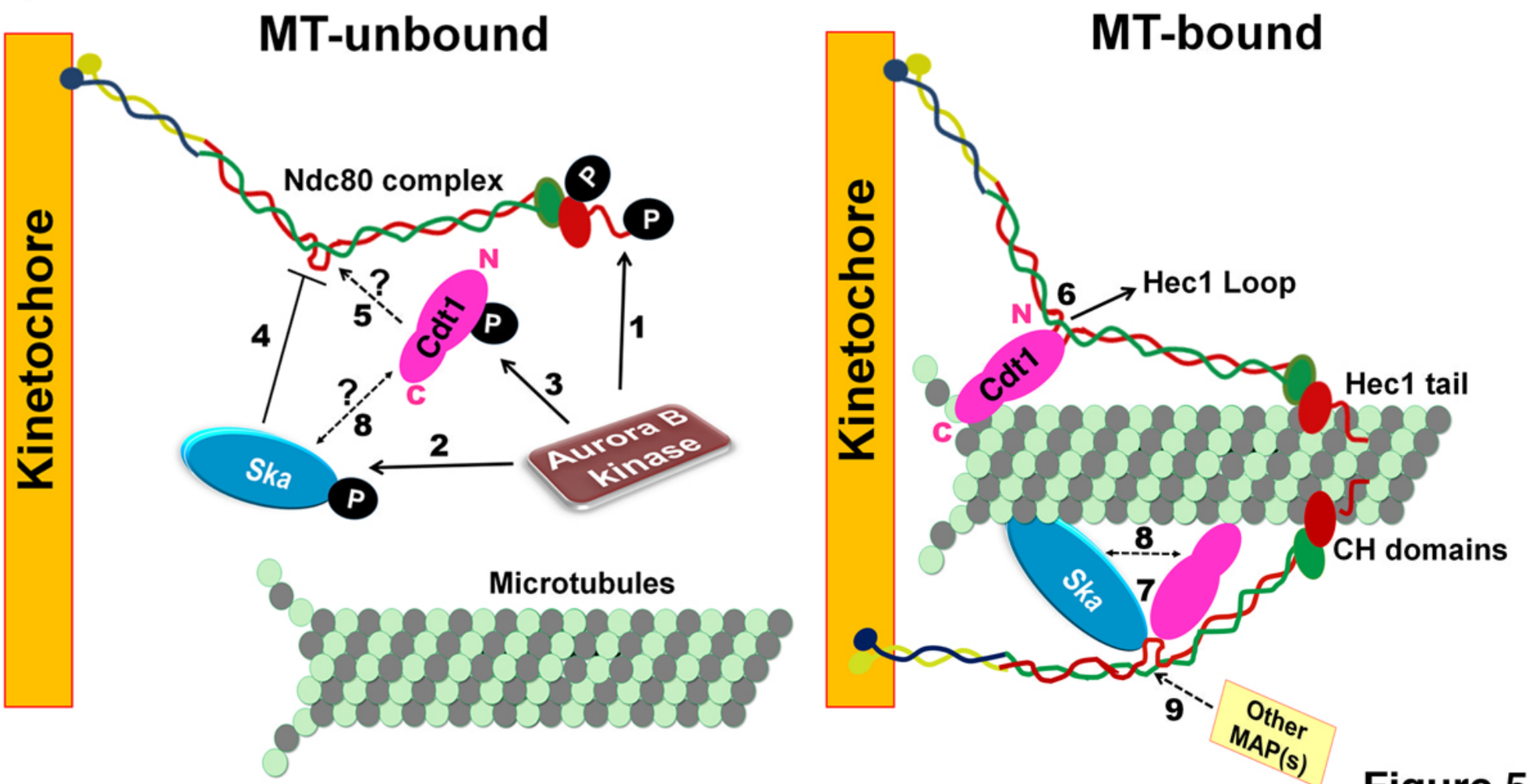

Figure 5